Transport coefficients for shape degrees in terms of Cassini ovaloids

F. A. Ivanyuk,[1,2] H. Hofmann,[1] V. V. Pashkevich,[3] and S. Yamaji[4]
[1]*Physik-Department der Technischen Universität München, D-85747 Garching, Germany*
[2]*Institute for Nuclear Research of the Ukrainian Academy of Sciences, Kiev-28, Ukraine*
[3]*Joint Institute for Nuclear Research, 141980 Dubna, Russia*
[4]*Cyclotron Laboratory, Riken, Wako, Saitama, 351-01, Japan*
(Received 10 July 1996)

Previous computations of the potential landscape with the shapes parametrized in terms of Cassini ovaloids are extended to collective dynamics at finite excitations. Taking fission as the most demanding example of large scale collective motion, transport coefficients are evaluated along a fission path. We concentrate on those for average motion, namely, stiffness C, friction γ, and inertia M. Their expressions are formulated within a locally harmonic approximation and with the help of linear response theory. Different approximations are examined and comparisons are made with both previous studies, which involved different descriptions of single-particle dynamics, and macroscopic models. Special attention is paid to an appropriate definition of the deformation of the nuclear density and its relation to that of the single-particle potential. For temperatures above 3 MeV the inertia agrees with that of irrotational flow to less than a factor of 2, but shows larger deviations below, in particular in its dependence on the shape. Also, friction exhibits large fluctuations along the fission path for small excitations. They get smoothed out above 3–4 MeV where γ attains values in the range of the wall formula. For $T \geqslant 2$ MeV the inverse relaxation time $\beta = \gamma/M$ turns out to be rather insensitive to the shape and increases with T. [S0556-2813(97)01304-6]

PACS number(s): 21.60.Ev, 21.60.Cs, 24.10.Pa, 24.75+i

I. INTRODUCTION

One of the oldest but still most challenging problems of nuclear physics is an adequate description of collective motion at finite excitations. As the prime example one may quote nuclear fission which has attracted the attention of both experimentalists as well as theoreticians since its discovery. To date it is still an open question which type of configurations the system undergoes on its way from the potential minimum over the saddle region down to scission. Whereas in the early days those of the compound model were clearly favored in theoretical pictures, after the discovery of the shell model that of independent particle motion came into fashion more and more. This development was enhanced after computers became fast enough such that Hartree-Fock type computations could be done in every laboratory.

However, there can be little doubt that this picture fails to describe collective motion at finite excitations where one is compelled almost by experimental evidence that the dynamics shows irreversible behavior, not only by the very nature of the decay process itself, but by the appearance of frictional forces. It is more than questionable that this feature can adequately be met by introducing simpleminded collision terms. Decent descriptions of fission in terms of the one-body density operator most likely require one to consider correlations beyond the independent particle picture, together with non-Markovian effects. This is a difficult problem in itself, not to mention the computational task of solving this equation of motion for the one-body density.

For these reasons it may still be interesting and worthwhile to start from a more phenomenological point of view, introducing the shape parameters as collective variables. It is true that in this way again the picture of independent particles will serve as a starting point, in the form of the deformed shell model. However, the latter is simple and flexible enough to allow one to consider residual interactions, in one way or another. As we shall see, it may be possible to gain insight into their importance by studying dynamical aspects. Likewise, we may be able to get information on the complexity of the configurations which are to be considered.

Such a task becomes more feasible in the case where collective motion is sufficiently slow. Then one may exploit the quasistatic picture which reduces the complexity of the full problem drastically. Under such circumstances one may actually linearize the problem and treat collective motion locally within a harmonic approximation. In this way one may take advantage of the benefits of linear response theory.

One of the major problems in theories of this type is to find a decent guess for the relevant macroscopic variables, a problem which is familiar almost from all transport theories. For nuclear fission there exists some kind of guiding principle through the liquid drop model. The latter is known to represent the static energy for temperatures above 1–2 MeV. Since at these temperatures one expects motion to be strongly damped, it will most likely follow somehow the line of steepest decent. Possible shapes which a fissioning nucleus may assume on its way to scission have been looked for in [1] by minimizing the liquid drop energy. This minimization has been done for some realistic energy density functional under the constraint of fixing a parameter which measures the distance between the evolving fragments. Incidentally, it is the same parameter which we are going to exploit later on in our approach. It so turns out that the shapes found in this way can be approximated fairly well by the Cassini ovaloids introduced to nuclear physics in [2]. Later in [3] a single-particle model has been constructed for such a parametrization of shapes, which was based on the Woods-Saxon potential.

In this paper we are going to use this model for computations of transport coefficients, after some suitable modifications which are necessary to incorporate the effects mentioned above. One of our goals will be to study average motion along the fission path for different temperatures, as it is reflected in the associated transport coefficients of inertia, friction, and local stiffness. In this sense the aim of our present work is similar to the one of [4], where a two-center shell model was used. The latter feature renders the previous model simpler on the computational level. On the other hand, the parametrization of the shape by means of Cassini ovaloids opens the possibility of treating more realistic shapes, which are perhaps better suited to describe the later stages of a fission process. Furthermore, it is fair to say that the Woods-Saxon potential may be supposed to resemble more the ''true'' mean field.

For Cassini ovaloids commonly a few parameters suffice to treat in simple terms a whole variety of realistic shapes including very compact ones as well as strongly deformed ones with a well-developed neck or even those corresponding to separated fragments. In this sense this parametrization may be considered superior to expansions in terms of spherical harmonics (see [5]). In the ideal case one would then be able to compute transport tensors for all the parameters, the collective degrees of freedom, one claims to be relevant. This is a tremendous task and so far has been carried through only for a two-dimensional model [6], without utilizing though the full microscopic potential of linear response theory. In this paper we want to restrict ourselves to the one-dimensional case. The main reason for that is found, of course, in the simplification one gains by this restriction. However, it may be said that at present most of the applications of macroscopic equations of motion to fission at finite excitation adhere to a similar confinement; see, e.g., [7–10]. Evidently one then needs to rely on the ''right'' guess of the fission path. As said before and for arguments given there we presume it to be represented well enough by the line along the valley of the static energy. Possible improvements have to be left for future studies.

II. DEFORMED SHELL MODEL

A. Shape parametrization

We follow the suggestion put forward in [3], but would like to repeat the most important elements for convenience. The Cassini ovaloids are obtained by rotating the curve

$$\rho(z,\epsilon)=R_0[\sqrt{a^4+4\epsilon z^2/R_0^2}-z^2/R_0^2-\epsilon]^{1/2} \qquad (2.1)$$

around the z axis, with z and ρ being cylindrical coordinates. The constant a is defined by volume conservation, implying that the family of shapes Eq. (2.1), depends only on one deformation parameter ϵ. As is easily recognized from Eq. (2.1) the value of $\epsilon=0$ corresponds to a sphere. For $0<\epsilon<0.4$ the form resembles very much that of a spheroid with the ratio of the axes given by

$$\frac{\text{shorter axes}}{\text{longer axes}}=\frac{1-2\epsilon/3}{1+\epsilon/3}. \qquad (2.2)$$

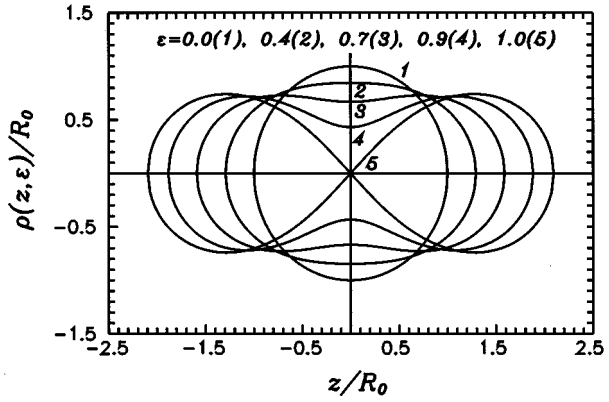

FIG. 1. The parametrization of the shape of the nuclear surface in terms of Cassini ovaloids. The values of the deformation parameter ϵ [see Eq. (2.1)] are indicated in the figure.

At $\epsilon\approx 0.5$ a neck appears and at $\epsilon=1.0$ the nucleus separates into two fragments. A few examples of the family (2.1) are shown in Fig. 1.

It is possible to describe a more general class of axially symmetric shapes by exploiting an expansion about the surface given by Eq. (2.1). We may introduce two new coordinates R and x such that $R=\text{const}=R_0$ corresponds to the Cassini ovals (2.1). The coordinate x specifies the position of a point on the line given by Eq. (2.1); see [3] for details. With these two variables at our disposal we may parametrize a new shape. The latter is meant to express the deviation from the ovaloid given by Eq. (2.1) by means of an expansion into a series of Legendre polynomials,

$$R(x)=R_0\left(1+\sum_n \alpha_n P_n(x)\right). \qquad (2.3)$$

The full set of collective variables or parameters then includes the coefficients α_n in addition to the ϵ from before.

Sometimes it is convenient to introduce a measure for the overall elongation of the nucleus instead of ϵ. One may chose, for instance, the distance R_{12} between the left and right center of masses. To have a dimensionless quantity one may divide R_{12} by the diameter $2R_0$ of the sphere (of identical volume) to get

$$r_{12}\equiv\frac{R_{12}}{2R_0}=\frac{\int|z-z_{\text{c.m.}}|dV}{R_0\int dV}, \qquad (2.4)$$

with $z_{\text{c.m.}}$ being the z coordinate of the center of mass of the the whole complex. The integration is carried out over the volume within the sharp surface specified by Eq. (2.3). Asymptotically, the r_{12} turns into half of the distance between centers of mass of the fission fragments. Incidentally, this variable is defined uniquely for any parametrization of the shape and has been used in the past by many authors. This feature facilitates comparisons to theories which are based on shell models with different shape variables. The relation between r_{12} and ϵ is demonstrated in Fig. 2.

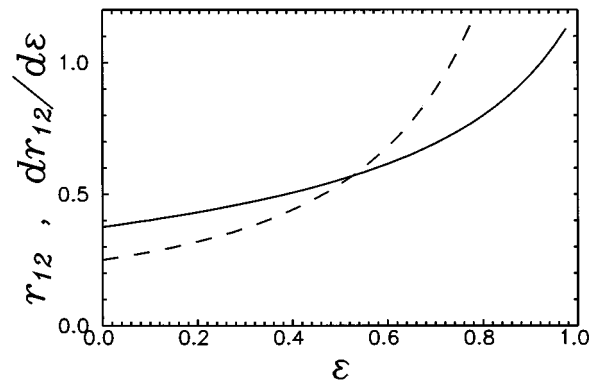

FIG. 2. The relation between r_{12} and ϵ (solid line); the derivative $dr_{12}/d\epsilon$ is shown by a dashed line.

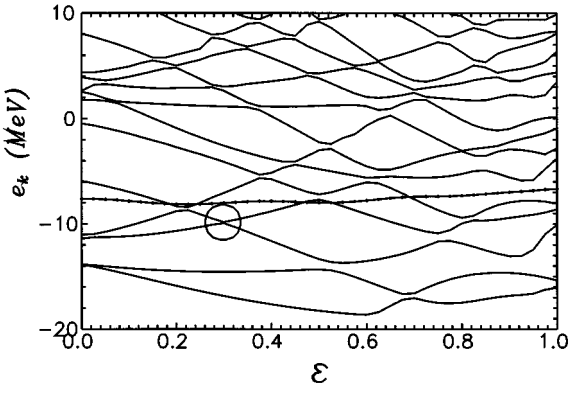

FIG. 3. The energies e_k of single-particle states (for a fixed z component of angular momentum and parity, $j_z^\pi = 3/2^-$) as functions of ϵ. The line with stars marks the position of the chemical potential computed for $T=1$ MeV. The circle marks the pseudocrossing which at $\epsilon=0.3$ is closest to the chemical potential; see text.

B. Single-particle Hamiltonian

The single-particle Hamiltonian $\hat{h}_{ipm}$ will be constructed as in [3]. It has terms for the kinetic energy $\hat{T}$, the radial potential $\hat{V}$, the spin-orbit coupling $\hat{V}_{\text{s.o.}}$, and the Coulomb potential $\hat{V}_{\text{Coul}}$:

$$\hat{h}_{ipm} = \hat{T} + \hat{V} + \hat{V}_{\text{s.o.}} + \hat{V}_{\text{Coul}}. \tag{2.5}$$

The radial part $\hat{V}$ is represented by a finite depth Woods-Saxon potential

$$V(\rho,z) = V_0\{1+\exp[l(\rho,z)/a]\}^{-1}, \tag{2.6}$$

where $l(\rho,z)$ is the shortest distance from the point (ρ,z) to the sharp surface and a is the diffuseness parameter which is assumed to be constant along the surface. The spin-orbit potential may be written in a way which makes apparent that it is proportional to the gradient of the potential given in Eq. (2.6),

$$\hat{V}_{\text{s.o.}} \propto [\vec{s},\vec{p}]\nabla V. \tag{2.7}$$

Here $\vec{p}$ and $\vec{s}$ stand for the nucleon's momentum and the spin. The Coulomb potential is calculated for a charge distributed uniformly inside the sharp surface (2.3) or (2.1).

The single-particle energies and wave functions are determined by diagonalizing the matrix of the Hamiltonian (2.5) calculated with the wave functions of a deformed axially symmetric oscillator potential; see [11]. An example of the deformation dependence of the single-particle energies is shown in Fig. 3. As the result of diagonalization one obtains not only energies and wave functions of bound states, but also those of discrete states of positive energy, which for the Woods-Saxon potential lies in the continuum. The density of these states depends on the number of oscillator shells included in the basis. In the computations within the shell correction method the number of oscillator shells is optimized by the requirement that the states with positive energies provide a smooth extrapolation of the density of bound states into the continuum. Accounting for such states with positive energy improves considerably the ''plateau'' of the shell correction as a function of the averaging interval. In the present paper we do so not only when calculating deformation energies but also in the computation of transport coefficients. The cutoff in the single-particle energy was set equal to 20 MeV. We have checked that a variation of the cutoff energy within the interval 5–20 MeV does not change much the values of the transport coefficients. This may be understood from the fact that these transport coefficients reflect the truly low frequency behavior of the system.

C. Deformation energy

The deformation energy E_{def} at zero temperature is calculated according to the shell correction method [12,13] as the sum of the liquid drop energy $E_{\text{def}}^{\text{LDM}}$ and the shell correction $\delta E^{n,p} + \delta P^{n,p}$ (including the one for the pairing energy):

$$E_{\text{def}} = E_{\text{def}}^{\text{LDM}} + \sum_{p,n} (\delta E^{p,n} + \delta P^{p,n}). \tag{2.8}$$

The liquid drop energy is computed as the contributions from the Coulomb E_{Coul} and surface E_S energies according to [12,13]

$$E_{\text{def}}^{\text{LDM}} = E_{\text{Coul}} + E_S - (E_{\text{Coul}}^0 + E_S^0), \tag{2.9}$$

where E_{Coul}^0 and E_S^0 are the corresponding energies of the spherical shape. As an example, Fig. 4 exhibits the results of the calculation of E_{def} and $E_{\text{def}}^{\text{LDM}}$ at zero temperature for ^{224}Th as a function of the parameters ϵ and α_3.

The temperature dependence of Coulomb and surface energy is accounted for by using the forms

$$E_{\text{Coul}}(T) = E_{\text{Coul}}(T=0)(1-\alpha T^2),$$

$$E_S(T) = E_S(T=0)(1-\beta T^2), \tag{2.10}$$

with $\alpha = 0.000\,763\ \text{MeV}^{-2}$ and $\beta = 0.005\,53\ \text{MeV}^{-2}$ [14]. To compute the shell correction at finite temperature we use the phenomenological ansatz proposed in [5]:

$$\delta E(T) + \delta P(T) = [\delta E(0) + \delta P(0)]\frac{\tau}{\sinh\tau}, \tag{2.11}$$

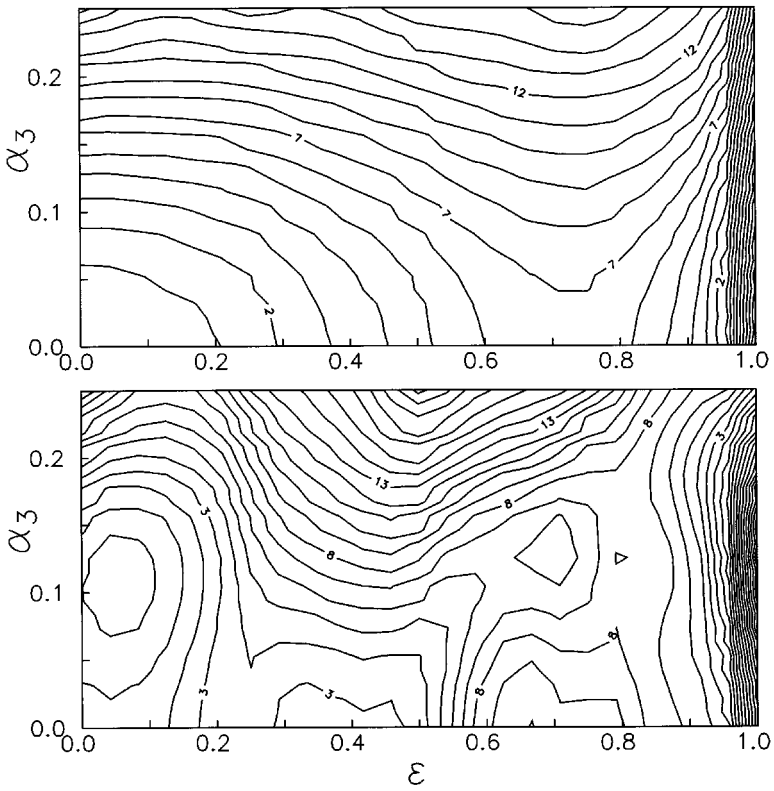

FIG. 4. The liquid drop (top) and total (bottom) deformation energies of ^{224}Th at $T=0$ as a function of ϵ and α_3.

with $\tau=2\pi^2 T/\hbar\omega_0$ and $\hbar\omega_0=41A^{-1/3}$, A being the mass number of the fissioning nucleus.

For temperatures larger than 1 MeV (as considered in the present paper) the shell effects are strongly suppressed. Already at $T=1$ MeV the minimum of the total deformation energy almost coincides with the bottom of the liquid drop valley. As said before the latter can be approximated rather well just by the Cassini ovaloids. Thus we restricted our set of deformation parameters to the one parameter ϵ only, with all the α_n put equal to zero. However, instead of ϵ we prefer to use r_{12} defined by Eq. (2.4). The r_{12} dependence of the total deformation energy and that of the liquid drop are shown in Fig. 5.

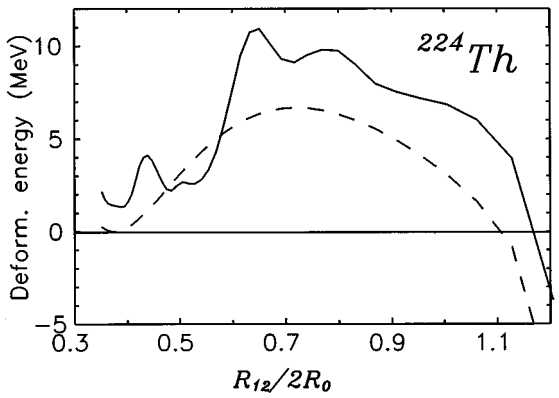

FIG. 5. The total (solid) and liquid (dashed) drop components of the deformation energy along the liquid drop fission valley for ^{224}Th.

III. DYNAMICS IN A LOCAL HARMONIC APPROXIMATION

In the following we will assume to be given a many-body Hamiltonian $\hat{H}(\hat{x}_i,\hat{p}_i,Q(t))$ which depends parametrically on the collective variable Q which specifies the shape of the nuclear surface. Although for the computations to be presented below it will mostly be identical to r_{12}, in this section we still prefer to use the general notation Q instead, last but not least to indicate the general validity of the discussion to come. This Hamiltonian is assumed to represent the system's total energy. On the level of the shell model this means adding some c-number terms to the sum over those single-particle Hamiltonians introduced in Eq. (2.5) (see [15]). As will be discussed in the next section, later on we want to account for collisional damping, which from a principal point of view requires adding a two-body interaction $\hat{V}^{(2)}_{\rm res}(\hat{x}_i,\hat{p}_i)$. For the moment it is not very important to know details about the way it will be handled, besides the fact that we claim this interaction to be independent of Q.

As a consequence of the latter feature, the generator for collective motion, namely,

$$\partial\hat{H}(\hat{x}_i,\hat{p}_i,Q)/\partial Q\equiv\hat{F}(\hat{x}_i,\hat{p}_i,Q),$$

is of pure one-body nature. This operator defines the main source of the coupling between the collective degree of freedom $Q(t)$ and the nucleonic ones. Indeed, within the local harmonic approximation (LHA) the effective Hamiltonian can be written as

$$\hat{H}(Q)=\hat{H}(Q_0)+(Q-Q_0)\hat{F}+\frac{1}{2}(Q-Q_0)^2\left\langle\frac{\partial^2\hat{H}}{\partial Q^2}(Q_0)\right\rangle^{\rm qs}_{Q_0,T_0}. \quad (3.1)$$

In the second order term the ''nucleonic'' part appears only as an average of the corresponding operator. Consistently with the harmonic approximation, this average is to be built with that density operator $\rho_{\rm qs}(Q_0)$ which in the quasistatic picture is to be calculated with the Hamiltonian at Q_0, namely, $\hat{H}(Q_0)$. It is here where thermal concepts come into play. In this ''unperturbed'' density operator (for the nucleons) one needs to specify the amount of heat the nucleonic (or intrinsic) degrees of freedom have at the given configuration parametrized by Q_0. The simplest possibility is offered by the canonical distribution[1] $\rho_{\rm qs}(Q_0)\propto\exp[-\hat{H}(Q_0)/T]$, to which our computations will be restricted. Clearly this picture has to rely on the assumption of a quick relaxation of the relevant internal degrees of freedom; we will come back to this question later on.

Details about this LHA can be found in many references; see, e.g., [16–18]: There it is also described how this local dynamics can be handled within a suitable application of linear response theory. For this reason, we will only recall the most important theoretical issues.

A. Collective response function

The local motion in the Q variable can be described in terms of the so-called collective response function $\chi_{\rm coll}(\omega)$. It can be derived by introducing a (hypothetical) external force $\hat{F}\tilde{f}_{\rm ext}(t)$ and by evaluating how the deviation of $\langle\hat{F}\rangle_\omega$ from some properly chosen static value reacts to this external field in linear order:

$$\delta\langle\hat{F}\rangle_\omega=-\chi_{{\rm coll}(\omega)}f_{\rm ext}(\omega). \quad (3.2)$$

As shown in [17] and [16] the $\chi_{\rm coll}(\omega)$ can be brought to the form

$$\chi_{{\rm coll}(\omega)}=\frac{\chi(\omega)}{1+k\chi(\omega)}. \quad (3.3)$$

Here a response function $\chi(\omega)$ for ''intrinsic'' motion appears: The $\chi(\omega)$ measures how, at some given shape Q_0 and for some temperature T_0, the nucleonic degrees of freedom react to the coupling $\hat{F}\,\delta Q(\omega)$. Its time-dependent version reads

$$\tilde{\chi}(t-s)=\Theta(t-s)\frac{i}{\hbar}{\rm tr}\{\hat{\rho}_{qs}(Q_0,T_0)[\hat{F}(t),\hat{F}(s)]\}\equiv 2i\Theta(t-s)\tilde{\chi}''(t-s). \quad (3.4)$$

In this expression the time development of the field operators is defined by the same Hamiltonian $\hat{H}(\hat{x}_i,\hat{p}_i,Q_0)$ which appears in the density $\hat{\rho}_{\rm qs}$. The function $\tilde{\chi}''(t-s)$ on the right stands for the so-called dissipative part. In Fourier space the full response separates into real and imaginary parts like $\chi(\omega)=\chi'(\omega)+i\chi''(\omega)$, the $\chi'(\omega)$ sometimes being called the reactive part.

As one may guess from the very construction, the derivation of Eq. (3.3) relies on quasistatic properties of the nucleonic degrees of freedom. For instance, such properties appear in the coupling constant k which is to be determined from

$$-k^{-1}=\left(\frac{\partial^2E}{\partial Q^2}\right)_S+\chi(\omega=0)\equiv C(0)+\chi(0). \quad (3.5)$$

Moreover, the nucleonic degrees of freedom are assumed to behave ergodic in the sense of having the adiabatic susceptibility $\chi^{\rm ad}=-\delta\langle\hat{F}\rangle/\delta Q|_S$ be identical to the isolated one, the static response $\chi(0)$:

$$\chi(0)=\chi^{\rm ad}. \quad (3.6)$$

As has been demonstrated in [18] this condition is not fulfilled in the deformed shell model, which implies that special measures are to be taken to which we will come to below.

It should be noted that the derivation of Eq. (3.3) involves a self-consistency relation between the deformation Q of the mean field and the one of the density. The latter may be measured by the expectation value $\langle\hat{F}\rangle_t$. For linearized dynamics this self-consistency condition reduces to the equation

$$k\langle\hat{F}\rangle_t=Q(t)-Q_0, \quad (3.7)$$

well known from the case of undamped vibrations [5,15]. Realize, that the quantity $\langle\hat{F}\rangle_t$ is to be calculated with the actual dynamical nuclear states accounting for their appropriate occupations.

Before concluding this subsection we like to write down a more convenient form for the stiffness $C(0)$ appearing in Eq. (3.5). It is defined as the second derivative of the internal energy $E(Q,S)$ with respect to deformation at fixed entropy S. Since it is not easy to calculate such a derivative, it is better to reexpress it by the one of the free energy f at fixed temperature [see Eqs. (A.18) and (A.19) of [17]]:

$$C(0)=\left(\frac{\partial^2f}{\partial Q^2}\right)_T+\left(\frac{\partial T}{\partial Q}\right)_S\frac{\partial^2f(Q,T)}{\partial Q\partial T}. \quad (3.8)$$

In [17] it was found that for temperatures larger than 1.5–2.0 MeV the change of T with the collective coordinate Q is small such that the second term on the right-hand side of Eq. (3.8) can be neglected. Below we would like to use the shell correction method when calculating static energies. In this method usually the intrinsic energy is involved, rather than the free energy. Thus one needs to relate the derivatives of the free and the intrinsic energy both taken at a fixed temperature. This can be done by differentiating the relation $E=f+TS$ with respect to deformation and obeying that the entropy can be expressed as $S=-(\partial f/\partial T)_Q$. As a result one gets

[1]For a discussion of the general problems of using the concept of temperature for an isolated system see [16].

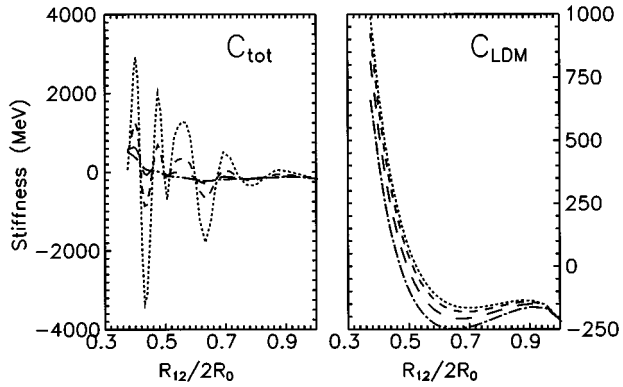

FIG. 6. The zero frequency limit (3.8) for the stiffness of the total (left) and liquid drop (right) static energies. The dotted, short-dashed, long-dashed, and dot-dashed lines correspond to temperatures $T=1$, 2, 3, and 4 MeV.

$$C(0)\approx\left(\frac{\partial^2 E}{\partial Q^2}\right)_T+T\frac{\partial}{\partial T}\left(\frac{\partial^2 f}{\partial Q^2}\right)_T\approx\left(\frac{\partial^2 E}{\partial Q^2}\right)_T. \tag{3.9}$$

As before, the expression on the right is justified for larger temperatures, where the change of $\partial^2 f/\partial Q^2$ with T is small. This approximation is used in the computations presented below. In Fig. 6 the stiffness (3.9) of the energy (2.8)–(2.11) is shown as function of the deformation parameter r_{12}. It is seen that its liquid drop part becomes negative for $r_{12}\geqslant 0.5$ and the total stiffness exhibits rather strong fluctuations due to shell structure.

B. Transport coefficients

In general the frequency dependence of $\chi_{\rm coll}(\omega)$ exhibits a complex structure. Its dissipative part $\chi''_{\rm coll}(\omega)$ represents the strength distribution over all possible modes of the whole nucleus which can be excited by an external force like the one introduced above, namely, $\hat{F}\tilde{f}_{\rm ext}(t)$. Rewriting Eq. (3.2) as

$$(\chi_{\rm coll(\omega)})^{-1}\delta\langle\hat{F}\rangle_\omega=-f_{\rm ext}(\omega), \tag{3.10}$$

it follows that the inverse of the collective response function can be interpreted as an integral kernel for the effective equation of motion for the time-dependent quantity $\delta\langle\hat{F}\rangle_t$. Evidently, this time-dependent form of the equation of motion must be expected to contain non-Markovian effects. However, there may be situations for which it becomes possible to reduce this complicated structure to differential form. The clue to this simplification can be found by recalling the case of the damped oscillator for which Eq. (3.10) takes the form

$$\begin{aligned}\chi_{\rm osc}^{-1}(\omega)\,\delta\langle\hat{F}\rangle_\omega&=(-M^F\omega^2-\gamma^F i\omega+C^F)\,\delta\langle\hat{F}\rangle_\omega\\&=-f_{\rm ext}(\omega).\end{aligned} \tag{3.11}$$

Here the following effective ''forces'' appear: an inertial one, a friction force, and the conservative one which is related to the derivative of the effective collective potential, calculated in linearized form. The associated ''transport coefficients'' have been marked by a superscript F to indicate that they are associated with the quantity $\delta\langle\hat{F}\rangle$.

Now the strategy of how to handle the general case is clear: Whenever there is a pronounced peak in the strength distribution $\chi''_{\rm coll}(\omega)$ we may approximate it by a Lorentzian. Since the latter is defined by three quantities, like the width, the position of the maximum, and its height, one may deduce the three transport coefficients which appear in the oscillator response, for instance, as given by Eq. (3.11). In principle, such a procedure may be applied to any one of the peaks of the original strength distribution, which allows one to deduce these transport coefficients for all the possible collective modes, the low frequency ones as well as the high frequency ones. As a matter of fact, such a scheme is commonly adopted for the description of collective vibrations, as discussed in [5,15]. The difference from the present application is seen in the fact that we want to apply this procedure to describe global dynamics in a local harmonic fashion. The latter aspect puts an additional constraint. As mentioned earlier, our application of linear response theory goes along with the assumption that collective motion is slow, such that the nucleonic degrees of freedom follow closely a thermal equilibrium. We may recall that in some formulas given above, this equilibrium has been parametrized by the quasistatic density operator $\hat{\rho}_{\rm qs}(Q,T)$. Estimates of the time scale on which such a relaxation can be expected to occur will be given below. But already on this level of information, it is clear that the whole concept would probably not work if high frequency collective modes were be important. For this reason we are bound to concentrate on low frequency ones, if the construction of the transport coefficients is to be consistent with the basic assumptions for the applicability of the quasistatic picture.

In practice the ''fit'' of the strength distributions of the oscillator model to the ''correct'' one involves the full response functions, not only their dissipative parts. In short such an adjustment may be characterized by $[\chi_{\rm coll}(\omega)]^{-1}\delta\langle\hat{F}\rangle_\omega\simeq[\chi_{\rm osc}(\omega)]^{-1}\delta\langle\hat{F}\rangle_\omega$. A more correct form can be written as a variational procedure

$$\delta\int_0^{\omega_{\rm max}}d\omega\left|k^2\chi_{\rm coll}(\omega)-\frac{1}{-M(\omega_1)\omega^2-i\gamma(\omega_1)\omega+C(\omega_1)}\right|^2=0, \tag{3.12}$$

with the variation to be performed with respect to the coefficients $C(\omega_1)$, $\gamma(\omega_1)$, and $M(\omega_1)$. In this way both real and imaginary parts of $\chi_{\rm coll}(\omega)$ are fitted simultaneously. Fortunately, for the practical applications to be discussed below it turns out that the coefficients $C(\omega_1)$, $\gamma(\omega_1)$, and $M(\omega_1)$ are rather insensitive to the upper integration limit $\omega_{\rm max}$. The value of the latter was fixed to be $\hbar\omega_{\rm max}=5$ MeV.

The reader will have noticed the appearance of the factor k^2 in Eq. (3.12), as well as the fact that we have left out the superscript F in the transport coefficients. This change is easily understood by referring to the self-consistency condition (3.7). The latter can be interpreted as a transformation from the F mode to the Q mode. It implies a corresponding transformation both for the response functions as well as for the transport coefficients (for details see [16]). In this sense

the $k^2\chi_{\rm coll}(\omega)$ and the transport coefficients $\mathcal{T}=M,\gamma,C$ stand for the collective response and the coefficients of the Q mode, respectively, with $\mathcal{T}^F=k^2\mathcal{T}$.

It may turn out that collective motion is so slow, as compared to the dynamics of the nucleons, that the transport coefficients can be deduced by expanding the response functions around $\omega=0$. At first such a procedure has been applied to the intrinsic response (cf. [19]). In this way one may get an approximate solution of the secular equation for the position of the poles of the collective response (3.3). One may write

$$\frac{1}{k}+\chi(\omega)\approx\left(\frac{1}{k}+\chi(0)\right)+\omega\left(\frac{\partial\chi}{\partial\omega}\right)_{\omega=0}+\omega^2\left(\frac{1}{2}\frac{\partial^2\chi}{\partial\omega^2}\right)_{\omega=0}=0. \tag{3.13}$$

This form invites us to define coefficients for friction $\gamma(0)$ and inertia $M(0)$ by

$$\gamma(0)=-i\frac{\partial\chi(\omega)}{\partial\omega}\bigg|_{\omega=0}=\frac{\partial\chi''(\omega)}{\partial\omega}\bigg|_{\omega=0} \tag{3.14}$$

and

$$M(0)=\frac{1}{2}\frac{\partial^2\chi(\omega)}{\partial\omega^2}\bigg|_{\omega=0}=\frac{1}{2}\frac{\partial^2\chi'(\omega)}{\partial\omega^2}\bigg|_{\omega=0}, \tag{3.15}$$

which in the past have been called the coefficients in the ''zero frequency'' limit. The effective stiffness $C(0)$ is seen to be identical to the local stiffness of the quasistatic energy [keep in mind Eq. (3.5)], as one would expect to hold true for slow motion, indeed. Incidentally, the expression for the inertia can be shown to be a generalization of the one of the cranking model to the case of damped motion [19]. Unfortunately, for strong damping this $M(0)$ becomes very small, and sometimes even negative. For practical applications this does not always lead to problems, as usually damping may be so strong that inertia must drop out of the macroscopic equations of motion. Nevertheless, this behavior of the inertia $M(0)$ is very unpleasant, but fortunately one can do better.

Rather than concentrate just on the denominator of Eq. (3.3), it is better to take into account the full information contained in this expression. As we may recall this was done implicitly when constructing the transport coefficients $M(\omega_1)$, $\gamma(\omega_1)$, and $C(\omega_1)$ by approximating Eq. (3.10) by Eq. (3.11). An equation like Eq. (3.11) may be obtained by expanding $[\chi_{\rm coll}(\omega)]^{-1}$ in Eq. (3.10) to second order in ω. In this way one gets

$$C\approx\frac{1}{k^2\chi_{\rm coll(\omega)}}\bigg|_{\omega=0}=\frac{\chi(0)+C(0)}{\chi(0)}C(0), \tag{3.16}$$

$$\gamma\approx\frac{1}{k^2}\frac{\partial(\chi_{\rm coll(\omega)})^{-1}}{\partial\omega}\bigg|_{\omega=0}=\frac{[\chi(0)+C(0)]^2}{\chi^2(0)}\gamma(0), \tag{3.17}$$

and

$$M\approx\frac{1}{2k^2}\frac{\partial^2(\chi_{\rm coll(\omega)})^{-1}}{\partial\omega^2}\bigg|_{\omega=0}=\frac{(\chi(0)+C(0))^2}{\chi^2(0)}\left(M(0)+\frac{\gamma^2(0)}{\chi(0)}\right). \tag{3.18}$$

As compared to the zero frequency limit defined above, there are two modifications: Whereas all three coefficients obtain a factor of proportionality, only the inertia gets an additional contribution. In most practical applications this proportionality factor is not very important, as usually the static response is much larger than the static stiffness: $\chi(0)\gg|C(0)|$. It is only for small excitations and for deformed oscillator shell models, in particular, that the size of $|C(0)|$ becomes comparable to that of $\chi(0)$. However, the additional term in Eq. (3.18) ensures that the modified inertia does not drop indefinitely anymore with increasing damping. Later on we will demonstrate with the help of numerical results that Eqs. (3.17) and (3.18) approximate the self-consistent friction $\gamma(\omega_1)$ and inertia $M(\omega_1)$ very well at temperatures $T\geqslant 2$ MeV. To distinguish from the zero frequency limit (3.14) and (3.15) we will associate the approximation (3.17) and (3.18) to ''the zero frequency limit for the collective response function.''

Finally, we should like to mention that relations similar to the ones given in Eqs. (3.16)–(3.18) were obtained earlier in [20], namely, for the model case that the collective response function just consists of one (approximately Lorentzian) peak. Solving the equations for $C(0)$, $\gamma(0)$, and $M(0)$ given in [20] with respect to C, γ, and M one gets Eqs. (3.16)–(3.18).

C. Transformation to sharp densities

In the previous section we found microscopic expressions of transport coefficients for large scale motion. For many reasons it is desirable to compare them with those of ''macroscopic models'' [21], such as the liquid drop model for the inertia and the wall formula for dissipation—not to mention stiffness, which we have seen to become identical to the one of the static energy anyway, as soon as collective motion becomes sufficiently slow. In [18] many points of the principal nature have been clarified about how the macroscopic limit can be obtained in microscopic theories, concentrating largely on vibrations around stable configurations. Here we like to look at another, more practical, albeit very important issue.

By its very nature, these macroscopic models assume the nuclear density to be constant inside some surface at which the density drops from the nuclear matter value down to zero within the zero range. Commonly this surface is parametrized with the same set of shape variables which in our description define the deformation of the mean field, for which in the present discussion we have chosen the one collective coordinate Q. Contrary to the macroscopic picture, the microscopic calculation leads to a density distribution with a soft surface, which in addition depends essentially on the occupation of states. Take the simple case of a spherical potential: If a shell with fixed angular momentum l is not filled completely, the corresponding density distribution will not be spherically symmetric. On the other hand, it is clear

that the transport coefficients $\mathcal{T}$ will depend sensibly on the distribution of matter. Thus one needs to employ some specific transformation to relate them from one case to the other. This is best done looking at the mean value (or moment) of the operator $\hat{F}$, as a representative for the average density.

In the case of our microscopic picture, we have seen the self-consistency condition (3.7) to imply the relation $\mathcal{T}^F = k^2 \mathcal{T}$ between the transport coefficients of the F and Q modes. All we need to do is to search for a similar condition which translates the F motion into that of the sharp density distribution, with the latter being expressed through the corresponding shape parameter. Such a relation can be found by applying the hypothesis, which we will substantiate below, that the average $\langle F \rangle_{\rm sharp}$, calculated with a density distribution having a sharp surface, can be approximated well by applying an appropriate Strutinsky smoothing to the shell model density. The latter is defined as

$$\langle F \rangle_{\rm sharp} \approx \sum_j F_{jj} \tilde{n}_j , \tag{3.19}$$

where the $\tilde{n}_j$ are smoothed occupation numbers [12,13]. How they may be used not only to calculate static expectation values as in Eq. (3.19), but of corresponding response functions as well has been studied in [22] and [18]. The desired relation between $\langle F \rangle_{\rm sharp}$ and Q may now be obtained simply by applying to Eq. (3.19) the derivative with respect to Q. One finds

$$\frac{\partial \langle \hat{F} \rangle_{\rm sharp}}{\partial Q} \approx \frac{\partial}{\partial Q} \sum_j F_{jj} \tilde{n}_j = \sum_{jk} \frac{\tilde{n}_j - \tilde{n}_k}{\epsilon_j - \epsilon_k} |F_{jk}|^2 + \sum_j \frac{\partial \tilde{n}_j}{\partial Q} \frac{\partial \epsilon_j}{\partial Q} \equiv -\chi^\gamma , \tag{3.20}$$

which may be used to deduce $\mathcal{T}_{\rm sharp} = (\chi^\gamma)^2 \ \mathcal{T}^F_{\rm sharp}$. Here, $\mathcal{T}_{\rm sharp}$ represents the transport coefficients for the sharp density distribution, but calculated for the associated Q mode. Combining this relation with the previous one, we get

$$\mathcal{T}_{\rm sharp} = (\chi^\gamma)^2 \mathcal{T}^F_{\rm sharp} \approx (\chi^\gamma)^2 \mathcal{T}^F(\omega_1) = (k\chi^\gamma)^2 \mathcal{T}(\omega_1). \tag{3.21}$$

As the only one further approximation we have assumed that both density distributions lead to the same averaged value of the field operator $\hat{F}$. In Eq. (3.21) there appear on the very left and on the right the transport coefficients for the Q mode, once for the sharp surface of the macroscopic models and once for the collective coordinate specifying the mean field. We may add here that the quantity χ^γ has a physical meaning similar to that of a static susceptibility, hence the choice of this symbol. The only difference from the isothermal susceptibility is found in using the smoothed occupation numbers $\tilde{n}_j(e_j)$ instead of $n_j(e_j;T)$.

Let us turn now to ''prove'' the hypothesis made. This can be done explicitly for the simple case of the deformed oscillator potential. For the more general case we want to appeal to physical intuition, to the extent of accepting the idea that by its very construction Strutinsky smoothing commonly does lead to the macroscopic picture.

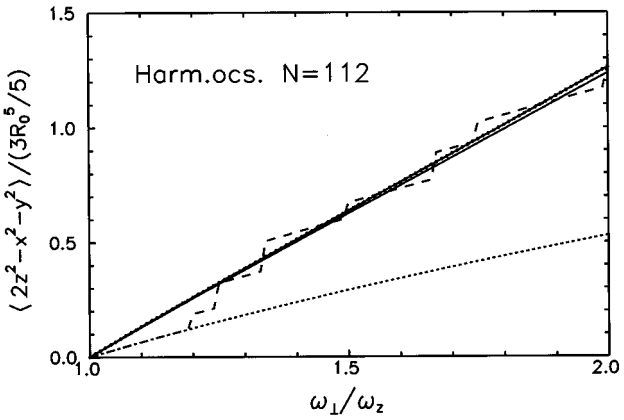

FIG. 7. A demonstration of the problem of consistency between the deformation of potential and density, exemplified at the deformed oscillator; for details, see text.

Suppose we are given a spheroid whose deformation Q is fixed by the ratio between the semiaxes in the z direction and the one perpendicular to it: $Q = z_0/y_0 = \omega_\perp/\omega_z$. The sharp surface S is then given by

$$\frac{x^2+y^2}{y_0^2} + \frac{z^2}{z_0^2} = 1. \tag{3.22}$$

The deformation of the sharp density may be classified by the average of the quadrupole operator $\hat{Q}_2(\vec{r}) = 2z^2 - x^2 - y^2$ calculated as

$$\langle Q_2 \rangle_{\rm sharp} = \int Q_2(\vec{r}) \rho_0(\vec{r}) d\vec{r} = \frac{2A}{5}(z_0^2 - y_0^2). \tag{3.23}$$

Here, $\rho_0(\vec{r})$ measures the density of homogeneous nuclear matter representing A nucleons distributed uniformly within this surface. In Fig. 7 the quadrupole moment (3.23) is plotted by the line with stars as function of the deformation parameter $Q = \omega_\perp/\omega_z$.

Conversely, the surface (3.22) may be interpreted as an equipotential surface of the corresponding deformed oscillator potential.[2] For such a potential one may compute single-particle wave functions $\varphi_i(\vec{r})$ and from them the moment of the microscopic density as

$$\langle Q_2 \rangle_{\rm dens} = \int Q_2(\vec{r}) \sum_j n_j |\varphi_j(\vec{r})|^2 d\vec{r}. \tag{3.24}$$

Obviously this moment $\langle Q_2 \rangle_{\rm dens}$ depends on the occupation numbers n_j. In Fig. 7 we show curves corresponding to three choices of n_j: Dotted line: the occupation numbers are fixed at the spherical shape, where the lowest energy states are filled, and kept constant, independent of Q (''diabatic'' situation). Dashed curve: at each crossing of states the particles and holes are redistributed in such a way that always the lowest states are occupied (''adiabatic'' situation). Solid

[2]For this case the quadrupole operator $\hat{Q}_2$ would be related to our field operator $\hat{F}$ taken at spherical shape by $F|_{Q=1} = -\frac{1}{3} m\omega_0^2 \hat{Q}_2$.

curve: here, the smoothed occupation numbers of the shell correction method are used. We see that for the diabatic occupation numbers the quadrupole moment (3.24) differs substantially from that of the sharp density distribution $\langle Q_2\rangle_{\rm sharp}$ (line with stars), approximately by a factor of 2. Recall that this sharp density distribution reflects the deformation of the potential.

On the contrary, the density computed with the adiabatic occupation numbers follows the deformation of the potential *on average*. It can be said that this feature is one of the basic elements of the Copenhagen picture of collective motion [5] (see also [15]). Indeed, such a redistribution of particles leads to a consistency between the shapes of the potential and the density. For static situations, this leads to the well-known relation between the occupation numbers in the various directions and the corresponding frequencies of the potential. In the treatment of [5] this relation is fulfilled for specific deformations. In Fig. 7, the latter correspond to the points where the dashed line crosses that with the stars. For this dashed line it is hardly possible to define precisely the derivative of $\langle Q_2\rangle_{\rm dens}$ with respect to the deformation parameter. On the other hand, the condition just mentioned can be fulfilled everywhere using the Strutinsky smoothed occupation numbers. In this way the derivative is well defined. Furthermore, the quadrupole moment of the density computed with the smoothed occupation numbers practically coincides with that of the sharp surface distribution.

IV. MICROSCOPIC INPUT

In this section we are going to specify further details of our treatment of nucleonic dynamics. It has already been mentioned that the mere shell model is not sufficient. At finite excitations the effects of collisions cannot be neglected; one even expects them to become the more important the higher the nucleonic temperature will be. To treat collisions on the basis of an explicit form of a two-body interaction $\hat V^{(2)}_{\rm res}(\hat x_i,\hat p_i)$ is hardly possible. Therefore we follow another path and parametrize the effect it would have on the single-particle energies. Details of this method can be found in the publications mentioned before, in particular in [16] (see also [23,24,18]).

A. Intrinsic response function

The Fourier transform of the intrinsic response function given in Eq. (3.4) can be expressed as the sum over single-particle states,

$$\chi(\omega)=\sum_{jk}\chi_{jk}(\omega)|F_{jk}|^2, \tag{4.1}$$

with

$$\chi_{jk}(\omega)=-\int_{-\infty}^{\infty}\frac{d\Omega}{2\pi\hbar}n(\Omega)[\varrho_k(\Omega)\mathcal{G}_j(\Omega+\omega+i\epsilon) +\varrho_j(\Omega)\mathcal{G}_k(\Omega-\omega-i\epsilon)]. \tag{4.2}$$

Here $n(x)$ is the Fermi function determining the occupation of single-particle levels. The $\varrho_k(\omega)$ represents the distribution of single-particle strength over more complicated states. It may be parametrized by

$$\varrho_k(\omega)=\frac{\Gamma(\omega)}{[\hbar\omega-e_k-\Sigma'(\omega)]^2+(\Gamma(\omega)/2)^2} \tag{4.3}$$

in terms of the real and imaginary parts of the self-energy $\Sigma(\omega,T)=\Sigma'(\omega,T)-i\Gamma(\omega,T)/2$ which are assumed to have the following forms:

$$\Gamma(\omega,T)=\frac{1}{\Gamma_0}\frac{(\hbar\omega-\mu)^2+\pi^2T^2}{1+[(\hbar\omega-\mu)^2+\pi^2T^2]/c^2} \tag{4.4}$$

and

$$\Sigma'(\omega,T)=\frac{-c^2}{2\Gamma_0}\frac{(\hbar\omega-\mu)/\sqrt{c^2+\pi^2T^2}}{1+[(\hbar\omega-\mu)^2+\pi^2T^2]/c^2}. \tag{4.5}$$

Both are connected to each other by a Kramers-Kronig relation. The μ in Eqs. (4.4) and (4.5) is the chemical potential and the cutoff parameter c accounts for the fact that the imaginary part of the self-energy does not increase indefinitely when the excitations get away from the Fermi energy. In the present calculation we choose $\Gamma_0=33$ MeV and $c=20$ MeV. The $\mathcal{G}_k$ appearing in Eq. (4.2) is the one-body Green function

$$\mathcal{G}_k(\omega\pm i\epsilon)=\frac{1}{\hbar\omega-\epsilon_k-\Sigma'(\omega,T)\pm i\Gamma(\omega,T)/2}, \tag{4.6}$$

which is related to the spectral density ϱ_k by

$$\varrho_k(\omega)=i[\mathcal{G}_k(\omega+i\epsilon)-\mathcal{G}_k(\omega-i\epsilon)]. \tag{4.7}$$

Details about the evaluation of the integral in Eq. (4.2) are given in the Appendix.

For future purpose we want to use this form (4.2) of the response function and write down a more detailed expression for the friction coefficient in the zero frequency limit:

$$\gamma(0)=-\int\frac{d\hbar\Omega}{4\pi}\frac{\partial n(\Omega)}{\partial\Omega}\sum_{jk}|F_{jk}|^2\varrho_k(\Omega)\varrho_j(\Omega). \tag{4.8}$$

It is obtained (see [18]) by substituting Eqs. (4.1) and (4.2) into Eq. (3.14).

B. Problem of ergodicity

In Sec. III A it was mentioned that the condition of ergodicity, Eq. (3.6), is hard to fulfill in the deformed shell model. This statement refers to the study presented in [18], where it was shown that even collisional damping does not help, at least in the version as used to date. One important reason was seen to lie in the fact that our renormalized single-particle energies have the same degeneracies as those of the pure shell model. But these degeneracies are by far larger and happen much more often than one would expect for configurations of the compound nucleus. If one believes the latter to be important — which should be the case for a fissioning

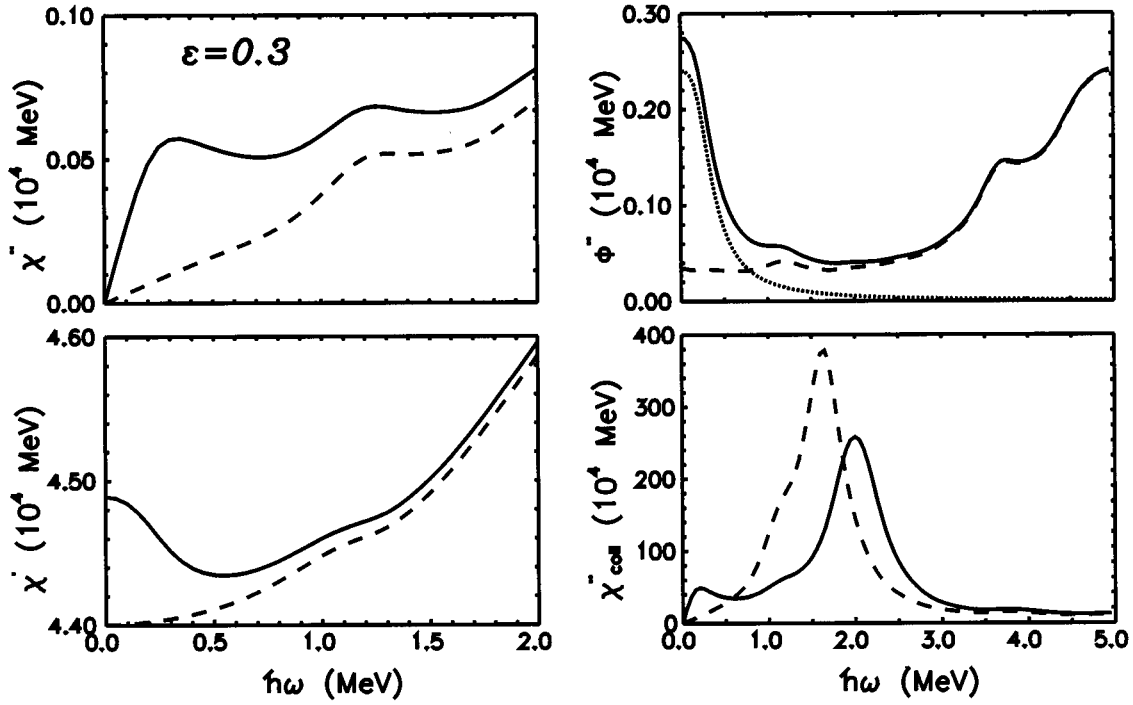

FIG. 8. The heat pole contribution to the relaxation and response functions, calculated at $T=1$ MeV.

system which has to overcome a large barrier — one needs to take special measures to cure the problem just mentioned.

One way to make the deficiencies apparent is to look at the heat pole which shows up either in the correlation function $\psi''(\omega)$ or in the relaxation function $\Phi''(\omega)$. Both are related to the dissipative response as

$$\chi''(\omega)=\frac{1}{\hbar}\tanh\left(\frac{\hbar\omega}{2T}\right)\psi''(\omega),$$

$$\Phi''(\omega)=\chi''(\omega)/\omega \tag{4.9}$$

(see [18] or [16] for more details as well as for references to the original literature). Both functions have a peak at $\omega=0$, whose width Γ_T was seen to be twice the single-particle width (4.4) calculated at the chemical potential, i.e., $\Gamma_T=2\Gamma(\omega=\mu,T)$. On very general grounds, the height of this peak can be seen to be proportional to the difference of isothermal and isolated susceptibilities, $\chi^T-\chi(0)$. Numerical calculations in [18] showed this height to be large. Rewriting this difference as $(\chi^T-\chi^{\rm ad})+[\chi^{\rm ad}-\chi(0)]$ and recalling that in the nuclear case the difference between the isothermal and adiabatic susceptibility, $(\chi^T-\chi^{\rm ad})$, is small [17,18], the origin is identified to come from a large violation of ergodicity: $\chi^{\rm ad}\neq\chi(0)$.

This discussion indicates what we can do to cure this problem: Cut the contributions of the heat pole to all functions mentioned previously down to the magnitude it would have in case the system were ergodic. This means to reduce the height of this peak at $\omega=0$ by the factor $(\chi^T-\chi^{\rm ad})/[\chi^{\rm ad}-\chi(0)]$. In [18] a system was studied were $\chi^T-\chi^{\rm ad}$ vanishes identically, such that the reduction of the heat pole amounted to neglecting contributions from all states having the same energy. Such a correction can easily be done. In expressions such as Eq. (4.1) one simply has to restrict the summations in a proper way. Here we like to adopt a similar procedure, in the sense of neglecting the influence of a finite difference $\chi^T-\chi^{\rm ad}$. At the temperatures considered it will be very small, indeed. On the other hand, we go one step further and neglect also contributions from neighboring states whose energy is finite but smaller than the collisional width of the particles, which as we just saw also reflects the width of the heat pole.

The consequences of such a manipulation are shown in Fig. 8 for the intrinsic response (left part), the corresponding relaxation function $\Phi''(\omega)$ (upper right part), and the collective strength distribution $\chi''_{\rm coll}(\omega)$ (lower right part). All of them have been computed for $T=1$ MeV. The solid lines correspond to calculations where all matrix elements are taken into account. For the dashed curves matrix elements F_{jk} between states of energy difference $|(e_k-e_j)|\leqslant\Gamma(\mu,T)$ have been discarded. Their contribution to the relaxation function is exhibited in the upper right part by the dotted line. This plot demonstrates nicely that the heat pole can be associated to a Lorentzian of width Γ_T around $\omega=0$, and thus corresponds to a pole on the imaginary axes [18,16].

It is interesting to note that for the present calculation 99% of this Lorentzian is made out only by two *pseudocrossings* of single-particle states which takes place close to the Fermi energy. By pseudocrossing we mean a situation where as a function of Q two levels come close but never cross; one such event is encircled in Fig. 3. The large contribution to friction in the zero frequency limit of Eq. (3.14) [or Eq. (3.17)] which results from this heat pole can be estimated looking at the upper right part of Fig. 8: The slope of the solid line is much larger than the one of the dashed line. On the other hand, contributions to $\gamma(0)$ from

real crossings of levels are very small. This is due to the fact that the matrix elements $|F_{jk}|$ vanish exactly at the crossing points and are very small in the vicinity of such a (real) crossing.

The influence of the heat pole (in the intrinsic system) on the collective strength distribution can be inferred from the lower right part of Fig. 8. The solid line shows a small peak at very small frequencies, say, $\hbar\omega \approx 0.2$–0.3 MeV. Compared to the much larger strength found in the peak at about 1.5–2 MeV one is inclined to just ''forget'' the small peak when one wants to define the transport coefficients. Indeed, it somehow looks very natural to associate the larger peak to the genuine low frequency mode. This may be understood as another argument for leaving out the contribution of the heat pole to the transport coefficients, besides the one involving ergodicity for intrinsic motion. All computations to be reported below were done along this line; i.e., contributions to the response function from the states with the energy difference $|(e_k - e_j)| \leqslant \Gamma(\mu, T)$ were not taken into account.

C. Influence of collisional damping on nucleonic relaxation

The whole formulation of our theory is based on the assumption that the nucleonic degrees of freedom stay close to a thermal equilibrium. The latter is not fixed, however; rather it continuously gets disturbed by collective motion itself, forgetting for the moment a possible evaporation of light particles or gammas. It should thus be of interest to have some estimate of an appropriate relaxation time. The best candidate for this is offered by the ''generator'' of collective motion, namely, the $\hat{F}(\hat{x}_i, \hat{p}_i, Q_0)$, which defines the coupling of the collective variable to the nucleons. It is predominately this quantity which ''decides'' which kind of modes of the intrinsic degrees of freedom get excited. We may recall from the discussion in Sec. III the close relation of this $\hat{F}$ to the nucleonic response function appearing in our theory: The $\chi(\omega)$ parametrizes that average ''excitation'' $\delta\langle\hat{F}\rangle_\omega$ which comes about through a change of the collective variable δQ. If we are just interested in estimating the time τ after which the $\delta\langle\hat{F}\rangle_t$ has decayed to its static value, we may study the time-dependent function $\widetilde{\chi}(t)$ given in Eq. (3.4). In a literal sense it represents the $\delta\langle\hat{F}\rangle_t$ if excited by a sharp pulse like $\delta Q(t) \propto \delta(t)$. Notice that for $t > 0$ the $\widetilde{\chi}(t)$ is proportional to the derivative of the Fourier-transformed relaxation function, namely, $\widetilde{\chi}(t) \propto d\widetilde{\Phi}''(t)/dt$ [see Eqs. (3.4) and (4.9)]. Thus the information contained in $\widetilde{\chi}(t)$ is equaivalent to that of $\Phi''(t)$ up to an additive constant. The latter measures the long time limit of $\Phi''(t)$; it is related to the strength of the heat pole. At the moment we are interested only in the behavior for finite times.

In Fig. 9 results of two different computations of $\widetilde{\chi}(t)$ are shown. One case just refers to the deformed shell model; for the other one, collisional damping is taken into account. It is clearly seen that only by way of such collisions may we speak of genuine relaxation. It is also observed that the latter does not depend much on the shape. However, the relaxation time τ decreases considerably with increasing temperature. The latter effect is expected of course from the very form by which the temperature appears in the single-particle widths (4.4). From the solid lines of Fig. 9 one may deduce for τ values like $(0.5, 0.3, 0.1)\hbar/\text{MeV}$ for $T = 1, 2, 5$ MeV. [This may, for instance, be done by approximating the envelope of $\widetilde{\chi}(t)$ by an exponential such that τ may be defined through the ''width'' at half maximum.] Later on in Sec. IV C we are going to compare them with typical time scales of collective motion, but we may say already here that this microscopic time τ is at least one order of magnitude smaller than the one which measures motion in the collective variable Q.

Finally, we should like to mention that the results found from the present computation are in accordance with those reported in [25].

V. NUMERICAL RESULTS FOR COLLECTIVE TRANSPORT COEFFICIENTS

In this section we will discuss the numerical results for transport coefficients $\mathcal{T}$ computed along the fission path of ^{224}Th. As was already mentioned, for temperatures above 1 MeV the fission path is parametrized in terms of Cassini ovaloids by only one deformation parameter ϵ. Since we prefer to use the parameter r_{12} instead of ϵ, we have to relate the transport coefficients accordingly. This can be done by exploiting the following relation, obeying that the α_n's are fixed:

$$\mathcal{T}_{r_{12}r_{12}} = \mathcal{T}_{\epsilon\epsilon}\left(\frac{dr_{12}}{d\epsilon}\right)^{-2}, \tag{5.1}$$

which simply follows from general properties of coordinate transformations. The derivative $\partial r_{12}/\partial\epsilon$ is obtained by differentiating Eq. (2.4); the result is shown by dashed line in Fig. 2. Recall that the deformation dependence of the transport coefficients is defined essentially by the choice of the collective variables. For example, $\mathcal{T}_{r_{12}r_{12}}$ decreases with r_{12} but $\mathcal{T}_{\epsilon\epsilon}$ increases as a function of ϵ. Both in the figures as well as in the text below we will omit the indices $r_{12}r_{12}$, keeping in mind that the transport coefficients are defined with respect to r_{12} (even if sometimes they will be shown as function of ϵ).

A. Accuracy of the zero frequency limit for the collective response function

The friction coefficient $\gamma(\omega_1)$ and mass parameter $M(\omega_1)$ defined according to Eq. (3.12) are shown in Fig. 10 by solid lines as function of the deformation parameter r_{12} for temperatures between 1 and 3 MeV. They are compared with calculations for which the approximation (3.17) and (3.18) is used for friction and inertia, respectively. The latter results are marked by dashed curves. As can be seen, this approximation is quite accurate for $T \geqslant 2$ MeV. This implies that for such temperatures one may avoid the time-consuming computation of the frequency dependence of the collective response function. One may compute friction and inertia directly from Eqs. (3.17) and (3.18). As for the large fluctuations seen at $T = 1$ MeV we expect them to become much smaller as soon as pairing correlations are taken into account, which shall be the subject of future studies.

For comparison we also show in Fig. 10 (by the lines with stars) wall friction γ_{wf} and the inertia of irrotational flow. According to [26] wall friction γ_{wf} is proportional to the

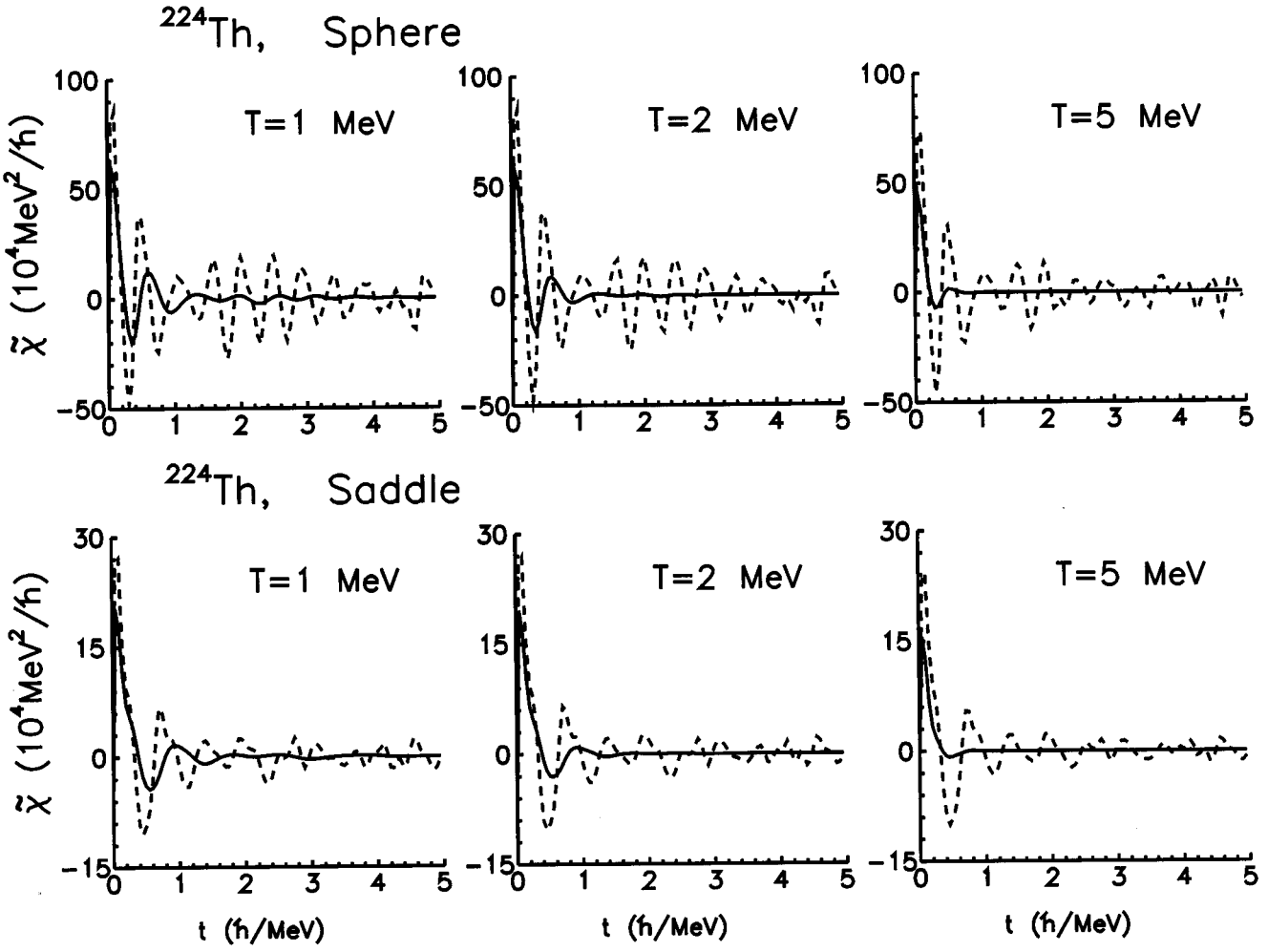

FIG. 9. The time-dependent function for the nucleonic response, calculated within the pure shell model (dashed curve) and for collisional damping (solid line).

squared normal velocity $u_n^2(s)$ of the surface, integrated over the nuclear surface. Following [26] this may be deduced from the loss of (collective) energy which is given by

$$\dot{E}=\frac{3}{4}\rho v_F \oint u_n^2(s)ds=\gamma_{\rm wf}\dot{r}_{12}^2(t), \tag{5.2}$$

where ρ and v_F are the nucleons' density and Fermi velocity. For axially symmetric shapes the surface velocity $u_n(s)$ can be expressed in terms of the profile function $\rho(z,\epsilon)$ from Eq. (2.1) as

$$u_n(z)=\overline{u_n}(z)\dot{r}_{12}(t),\quad \overline{u_n}(z)=\frac{1}{\Lambda(z)}\frac{\partial\rho}{\partial r_{12}},$$

$$\Lambda(z)=\sqrt{1+(\partial\rho(z,\epsilon)/\partial z)^2}. \tag{5.3}$$

The mass parameter of an incompressible irrotational fluid has been computed as suggested in [27]. It can be written as

$$M_{\rm irr}=m\oint \xi(s)\overline{u_n}(s)ds, \tag{5.4}$$

with the potential $\xi(\vec{r})$ for the velocity field expressed by the potential of some ''surface charge'' distribution

$$\xi(\vec{r})=\frac{1}{2\pi}\oint\frac{\nu(s')}{|\vec{r}-\vec{r}(s')|}ds'. \tag{5.5}$$

The substitution of Eq. (5.5) into the Neumann equation

$$\Delta\xi=0,\ (\vec{n}\nabla\xi)_S=u_n(s) \tag{5.6}$$

leads to some integral equation for the density of the ''surface charge'' $\nu(s)$ which was solved iteratively starting with

$$\nu^0(s)=-\overline{u_n}(s) \tag{5.7}$$

as a zeroth approximation to $\nu(s)$; for details see [27]. We have checked that for the particular case of the shape family (2.1) the Werner-Wheeler method [28] turns out to be a very accurate approximation to the mass parameter (5.4). Both results coincide within the thickness of the lines in the figure.

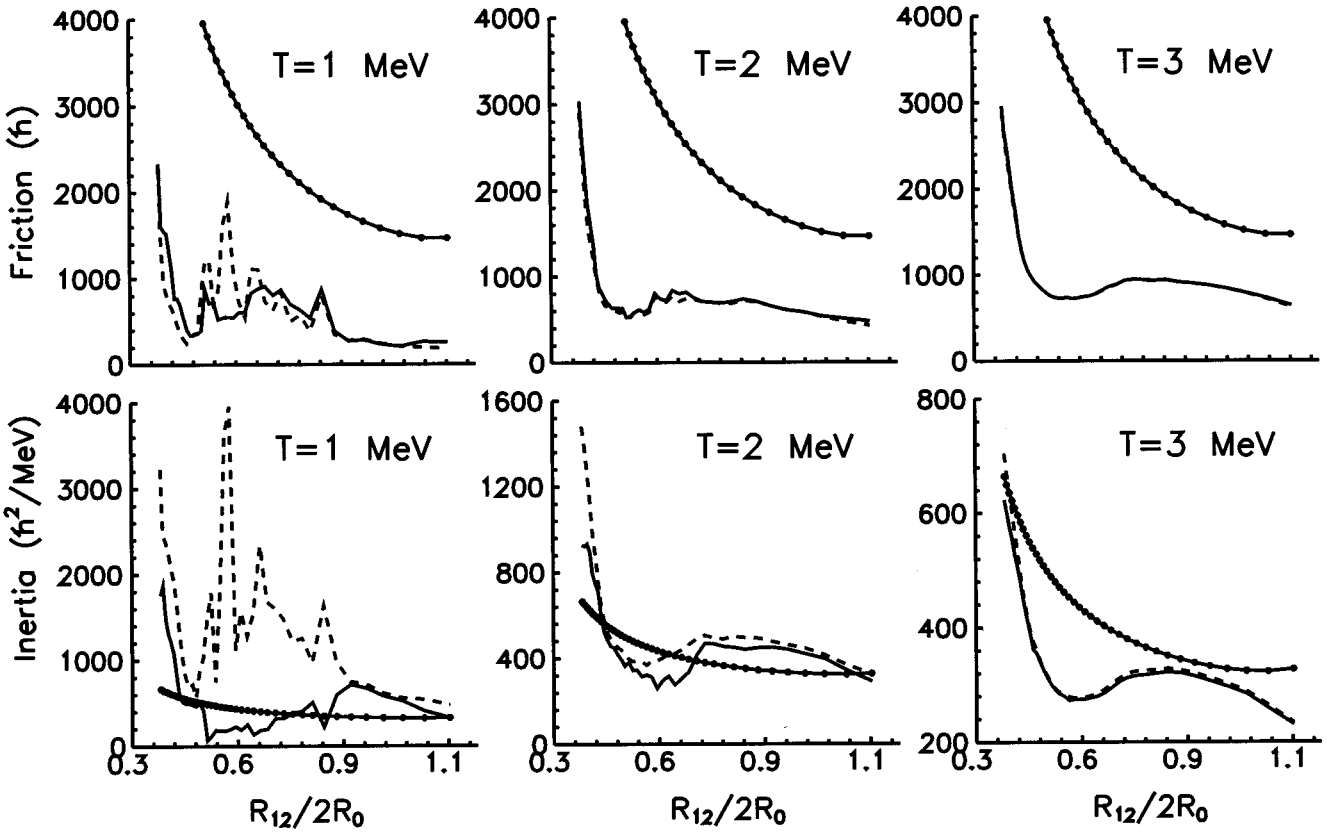

FIG. 10. The friction coefficient and the mass parameter at finite frequency (solid lines) and for the approximation (3.17) and (3.18) (dashed lines).

B. Temperature and deformation dependence of friction and inertia

In Figs. 11 and 12 the friction coefficient and the mass parameter are presented as a function of the deformation parameter ϵ for five different temperatures $T=1-5$ MeV. They have been calculated from the oscillator fit (3.12), but transformed to sharp densities according to Eq. (3.21). The parameter ϵ is chosen for reasons to be given below. In both figures results of the commonly adopted macroscopic models, namely, $\gamma_{\rm wf}$ and $M_{\rm irr}$, are shown by the lines with stars. Several observations can be made.

(i) To some extent the $\gamma_{\rm wf}$ and $M_{\rm irr}$ can be said to be reached at the higher temperatures. The very fact that this statement is more true for the inertia but less so for friction can be understood as follows. As shown in [18], $\gamma_{\rm wf}$ may be considered the macroscopic limit of our model only if such subtleties as collisional damping are left out. Conversely, the high temperature limit of the inertia is related to the value of the energy weighted sum, and the latter is known to be associated to $M_{\rm irr}$. This is true at least when one treats vibrations within simple models (see [5,15] for the situations of $T=0$ and [30] at $T\neq 0$).

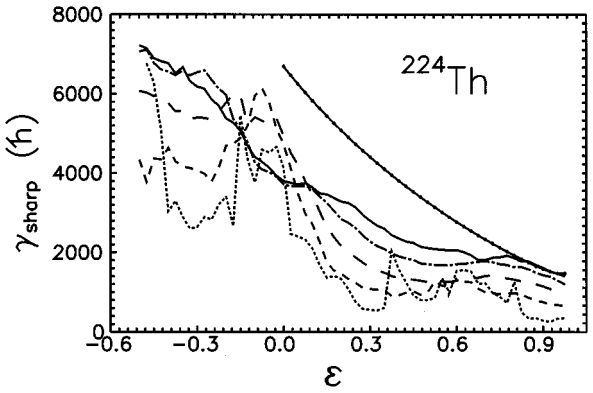

FIG. 11. The deformation dependence of friction; the dotted, short-dashed, long-dashed, dot-dashed, and solid lines correspond to temperatures $T=1$, 2, 3, 4, and 5 MeV.

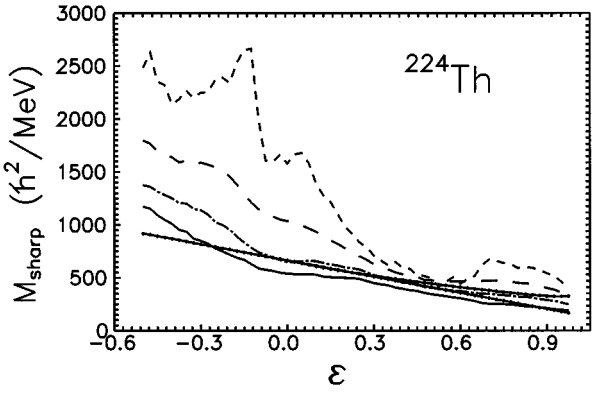

FIG. 12. The deformation dependence of the mass parameter for temperatures $T=1-5$ MeV. Different temperatures are marked by the same lines as in Fig. 11.

(ii) As has been demonstrated in [4], in the general case the evaluation of the sum rule value becomes somewhat delicate for collisional damping. The nice feature of reaching the $M_{\rm irr}$ automatically can be considered a proof of the usefulness of the transformation (3.21).

(iii) As in the calculations of [4], on average friction is seen to increase with T whereas the inertia decreases.

(iv) Again similarly to [4], both transport coefficients decrease with deformation on average.

(v) The coordinate dependence shows fluctuations around the average trend, which are more pronounced at smaller temperatures. They appear to be even larger than those reported in [4], but they are similar to the results of [29]. As for the friction coefficient, the dependence on deformation is particularly strong around the spherical shape. It reaches a kind of local maximum there or, perhaps, at a slightly oblate shape. These features can be exhibited more clearly for parametrization in terms of ϵ, for which reason we have made this choice here.

Many of these features point to the importance of shell effects, in particular the peak for friction around the spherical configuration, which is clearly visible for $T\approx 1-2$ MeV but which disappears at $T\approx 4-5$ MeV. We like to elaborate on this statement by trying to split the friction coefficient up into a smooth and a fluctuating part. For this study we take the zero frequency limit.

Let us suppose for a moment that the matrix elements $|F_{jk}|^2$ considered as a function of the single-particle energies have some smooth average component $\mathcal{F}^2(e,e')$ and the oscillating component can be neglected. In this case one may rewrite Eq. (4.8) in the form

$$\gamma(0)\approx -\hbar\pi\mathcal{F}^2(\mu,\mu)\int d\Omega\,\frac{\partial n(\Omega)}{\partial\Omega}g^2(\hbar\Omega). \quad (5.8)$$

The $\varrho_k(\Omega)$ in Eq. (4.8) are peaked functions with their maximum at $\hbar\Omega=\epsilon_k$ so that the sum of ϱ_k over k may be interpreted as the density $g(\hbar\Omega)$ of single-particle states. As usual the latter can be split into smooth and oscillating components $g(e)=\tilde{g}(e)+\delta g(e)$ with $\tilde{g}(e)=\langle g(e)\rangle$ and $\langle\delta g(e)\rangle=0$ where the brackets stand for an averaging over the single-particle spectrum. Inserting this decomposition into Eq. (5.8) and noting that an integration performed with the bell-like function $\partial n(\Omega)/\partial\Omega$ can be understood like the average introduced above, we will get

$$\gamma(0)\approx\hbar\pi[\overline{g^2}(\mu)+\langle\delta g^2(e)\rangle_{e=\mu}]\mathcal{F}^2(\mu,\mu). \quad (5.9)$$

Assuming the oscillating component of the density to be periodic in the energy with some period $\hbar\Omega_0$ and amplitude δg_0, viz., $\delta g(e)=\delta g_0\sin 2\pi e/\hbar\Omega_0$, it is easy to convince oneself that $\langle\delta g^2(e)\rangle=(1/2)\,\delta g_0^2$. The quantity δg_0 is determined by the magnitude of the shell correction. It is a smooth function of particle number (see [31]) but still depends on deformation. It is maximal at that deformation where the shell structure is more pronounced. For the Woods-Saxon potential this happens to be so at the spherical shape. So it is due to the shell structure that the friction coefficient gains additional contributions around the sphere. For the case of the Woods-Saxon potential this specific feature seems to be responsible for the dip one sees in Fig. 10 both for friction as well as for the inertia around $r_{12}\approx 0.5$, even at the somewhat larger temperatures of 3 MeV. It may be said, however, that such a behavior is not seen in computations performed with the model of [4]. There the change of the friction coefficient with r_{12}, for instance, resembles more the smooth one given by the wall formula.

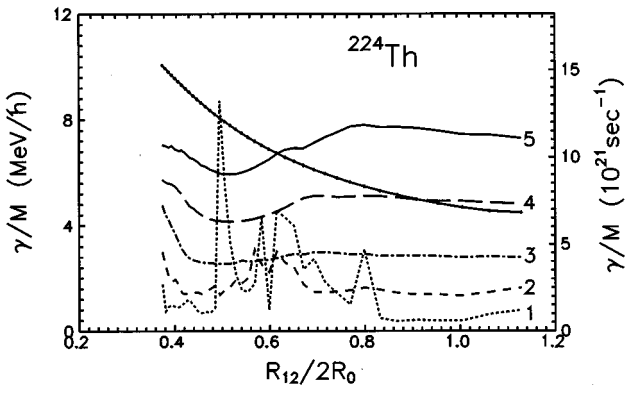

FIG. 13. The the inverse relaxation time $\beta=\gamma(\omega_1)/M(\omega_1)$ as a function of deformation and temperature (indicated in the figure).

C. Collective relaxation times

It has become customary to parametrize friction in terms of the ratio $\beta=\gamma/M$, although most interest has concentrated on friction alone; often the inertia was simply taken to be the reduced mass of the fissioning system. As we have seen above, for a microscopic theory both quantities will vary not only with the collective variable, but with temperature as well. It may be expected, of course, that for the ratio the dependence on shape is much weaker than that of the individual quantities. This follows simply from the observation that any common, purely geometrical factor will drop out. In Fig. 13 we present the results for β obtained from those for inertia and friction discussed before. Indeed, this quantity is essentially constant over the whole deformation region, for all computations but $T=1$ MeV, a case for which the fluctuations seen in our results are too large because of our neglecting pairing. However, there is a marked dependence on excitation: β increases strongly with T. This is in clear distinction to the result one gets from applying the wall formula for friction and that of irrotational flow for the inertia. Interestingly enough, these macroscopic estimates lead to some Q dependence, which in a sense is even larger than suggested by the trend of our results. It can be said that the latter are very close to those obtained in the computations with a two-center shell model potential [4].

Physically, the inverse of β can be interpreted as the relaxation time ($\tau_{\rm kin}=M/\gamma$) to the Maxwell distribution for collective motion. In full glory this feature can only be understood looking at the dynamics in collective phase space (see, e.g., [16]). However, one may grasp its content, recalling the local equation for average motion of the damped oscillator: $M\ddot{q}(t)+\gamma\dot{q}(t)+Cq(t)=0$. From this equation it also becomes apparent that yet another relaxation time can be defined, namely, $\tau_{\rm coll}=\gamma/|C|$. For overdamped motion the latter is the only relevant one. Actually, such a situation is given for temperatures above 1–2 MeV.

Let us infer this feature comparing the macroscopic relaxation times with the microscopic τ found in Sec. IV C. There we got values in the range $\tau=(0.3-0.1)\hbar/\mathrm{MeV}$ for temperatures between 2 and 5 MeV, discarding the case of $T=1$ MeV for the moment. Taking for the β of Fig. 13 typical values like 2 and 8 MeV/$\hbar$ for $T=2$ and 5 MeV, respectively, we recognize τ_{kin} to be comparable or only slightly larger than τ. This means that in this range of temperatures the friction force is so strong that it leads to an instant damping or disappearance of the kinetic energy. This is not in contradiction to the basic assumption behind the quasistatic picture. To justify the latter all one needs to have is the motion in Q to be slow compared to that for the intrinsic degrees of freedom. For this question it is the τ_{coll} which becomes relevant. Its value can be estimated with the help of Figs. 6 and 10. Let us concentrate on deformations for which the local stiffness does not get zero. Since for $T\geqslant 2$ MeV shell effects are not important anymore, we may estimate C as the one of the liquid drop energy. The right part of Fig. 6. tells us the $|C_{\mathrm{LDM}}|$ to be of the order of 150 MeV for r_{12} larger than about 0.6. In this range the value of γ is about $800\hbar$, as seen from Fig. 10 (for $T=2$ MeV; it is even larger for larger temperatures). For τ_{coll} this implies values of the order of $5\hbar/\mathrm{MeV}$, which are larger than τ by more than one order of magnitude.

VI. SUMMARY AND CONCLUSIONS

In this paper we have applied the single-particle model of [3] to describe large scale motion at finite excitations. To this end this model had to be modified to include effects of collisional damping and it had to be adapted to the formulation of collective motion in the spirit of the locally harmonic approximation (for a review see [16]). Numerical computations have been performed for the transport coefficients of average motion along a fission path. The latter was identified by the valley in the potential landscape obtained for the liquid drop model. It was argued that for the range of temperatures considered in the present study this path may be expected to represent fairly well the actual situation, first of all, because of the evidence one has from static considerations that Cassini ovaloids describe well the shapes of the fissioning nucleus. Second, for the large damping one expects to be given, the system will be creeping down the collective potential and thus will stay close to the line of steepest descent.

For the transport coefficients values were found which are in accordance with previous studies, in particular with the ones of [4]. This is especially so for their dependence on temperature and, to a lesser extent, for their variation with the nuclear shape. For instance, it turns out that typical effects of single-particle motion become more apparent here than they did in [4], as there are fluctuations of both friction and inertia with the collective variable. To a large amount they disappear when building ratios like for the $\beta=\gamma/M$ or the $\eta=\gamma/(2\sqrt{M|C|})$, two quantities which are commonly used to parametrize collective dynamics.

A new development has been achieved with respect to comparisons with macroscopic models, like that of irrotational flow for the inertia and that of wall friction. As one knows, both are calculated for sharp density distributions which may differ considerably from those which correspond to the nucleons' densities in the shell model. A transformation was suggested which allows one to connect both density distributions and thus enables one to connect the transport coefficients accordingly. This transformation was found by applying a Strutinsky smoothing procedure to evaluate the average static value of the relevant one-body operator $\hat{F}(\hat{x}_i,\hat{p}_i,Q_0)$. It is this operator which by a self-consistency argument is related to the deformation of the mean field.

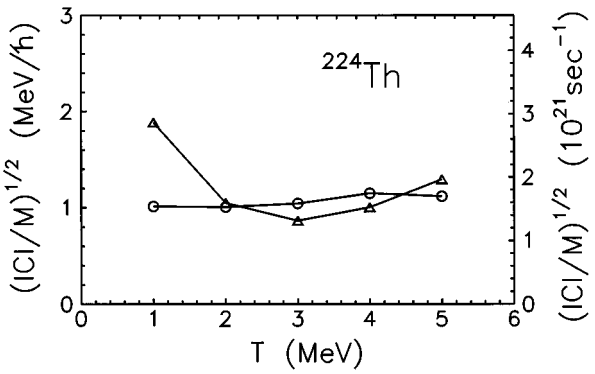

FIG. 14. The vibrational frequency $\varpi=\sqrt{|C|/M}$ as a function of temperature, calculated at the potential minimum (marked by circles) and at the saddle point (marked by triangles).

Finally, we briefly like to turn to comparisons with experimental findings. First of all, we may mention that the values for β shown above concur with the range suggested by fission experiments [32]. Two other relevant parameters are the $\varpi=\sqrt{|C|/M}$ and the η mentioned above, which, for instance, appear in Kramers' famous formula for the decay rate of a one-dimensional fission model: $R_{\mathrm{K}}=(\sqrt{1+\eta_s}-\eta_s)(\varpi_m/2\pi)\exp(-B/T)$. Here, B measures the barrier height, ϖ_m determines the vibrational frequency in the potential minimum, and η_s is to be evaluated at the saddle. The latter two quantities are shown in Figs. 14 and 15, respectively, for both points. They have been calculated by averaging the Q-dependent transport coefficients in the neighborhood of the minimum and the barrier, where both are those of the T-dependent potential energy. These results agree very well with those already shown in [4]. It is remarkable that

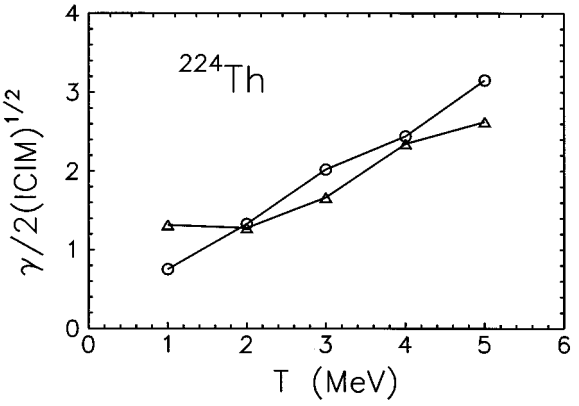

FIG. 15. The dimensionless parameter $\eta=\gamma/(2\sqrt{|C|M})$ as a function of temperature, calculated at the potential minimum (marked by circles) and at the saddle point (marked by triangles).

ϖ does not change much with T, neither at the minimum nor at the barrier. Conversely, like the β shown before, the η too definitely increases with temperature. This behavior is in at least qualitative agreement with the one found in [33] and the numbers for η lie in the range of values deduced only recently in [34] from experimental evidence. It is true, of course, that for more quantitative analyses one would have to consider both the effects of pairing as well as of angular momentum, not to mention the fact that there is some freedom [16] in adjusting the two parameters which define collisional damping. However, there is probably little doubt about the temperature dependence of our coefficients, say, above $T=1.5$–2 MeV. This marked change with T is in clear distinction to the macroscopic models mentioned. In the light of this feature agreements between experimental findings and theoretical descriptions appear somewhat questionable if they are only based on these macroscopic models [7,8]. Likewise the somewhat peculiar behavior of β with r_{12} suggested in [9] is not confirmed by our results (see also [4]). It is perhaps fair to say that some of the difficulties one still encounters at present when comparing theory with experiment are due to the high complexity of the problem itself as well that of the analysis of the data. To emphasize this statement, we would just like to take up a point raised in [10], namely, that common statistical codes evaluate the fission decay rate not by the transition state result, to which Kramers' formula reduces to for $\eta_s \to 0$, but by that of the ''statistical model'' where ϖ_m is replaced by T. The difference between these two variants can easily be inferred from Fig. 14.

ACKNOWLEDGMENTS

The authors want to thank the Deutsche Forschungsgemeinschaft for financial support. Two of us (F.A.I. and V.V.P.) would like to thank the Physics Department of the TUM for hospitality extended to them during their stay in Garching. This work was supported in part by the Deutsche Forschungsgemeinschaft.

APPENDIX: INTRINSIC RESPONSE FUNCTION

The computation of the intrinsic response function is somewhat involved. As a result of the frequency dependence of both the Fermi distribution $n(\omega)$ and width $\Gamma(\omega)$, the integral in Eq. (4.2) cannot be calculated analytically. The numerical integration is rather time consuming since $\varrho_k(\omega)$ are sharply peaked functions which width varies by two order of magnitude depending on the values of e_k. Fortunately the integration in Eq. (4.2) can be carried out by means of residues theorem closing the integration limit in the lower half plane. For this one needs to find the poles and residues of all the terms in the integrand of Eq. (4.2).

Let us first look for the poles of $\mathcal{G}_k(\omega+i\epsilon)$. Substituting Eqs. (4.3) and (4.4) into Eq. (4.6) and introducing the notation $\Delta \equiv \sqrt{c^2+\pi^2T^2}$, $\mu^{\pm}=\mu \pm i\Delta$, Eq. (4.6) can be brought to the form

$$\mathcal{G}_k(\omega+i\epsilon)=(\hbar\omega-\mu^+)(\hbar\omega-\mu^-) \times\left\{(\hbar\omega-e_k)(\hbar\omega-\mu^+)(\hbar\omega-\mu^-) +\frac{\hbar\omega-\mu^++i\Delta}{2\Gamma_0\Delta/c^4} +i\frac{(\hbar\omega-\mu^+)(\hbar\omega-\mu^-)-c^2}{2\Gamma_0/c^2}\right\}^{-1}. \quad \text{(A1)}$$

It is not difficult to note that the last terms in the second and third lines cancel each other and both the numerator and denominator can be divided by $\hbar\omega-\mu^+$. In this way $\mathcal{G}_k(\omega+i\epsilon)$ becomes

$$\mathcal{G}_k(\omega+i\epsilon)=\frac{\hbar\omega-\mu^-}{(\hbar\omega-\hbar\omega_k^+)(\hbar\omega-\hbar\omega_k^-)}, \quad \text{(A2)}$$

where $\hbar\omega_k^{\pm}$ are solutions of the equation

$$\left(\hbar\omega-e_k+i\frac{c^2}{2\Gamma_0}\right)(\hbar\omega-\mu^-)+\frac{c^4}{2\Gamma_0\Delta}=0, \quad \text{(A3)}$$

namely,

$$\hbar\omega_k^{\pm}=\frac{1}{2}\left[e_k+\mu^- -i\frac{c^2}{2\Gamma_0}\right] \pm\frac{1}{2}\left[\left(e_k-\mu^- -i\frac{c^2}{2\Gamma_0}\right)^2-\frac{2c^4}{\Gamma_0\Delta}\right]^{1/2}. \quad \text{(A4)}$$

Both poles of $\mathcal{G}_k(\omega+i\epsilon)$ lie in the lower half plane. The residues of $\mathcal{G}_k(\omega+i\epsilon)$ are simple functions of $\hbar\omega_k^{\pm}$ and μ^- as it is seen from Eq. (A2). From the definition (4.6) it is easy to see that poles and residues of $\mathcal{G}_k(\omega-i\epsilon)$ are complex conjugated to that of $\mathcal{G}_k(\omega+i\epsilon)$. The pole representation for $\varrho_k(\omega)$ is easily obtained from Eq. (A2). Besides the poles of $\mathcal{G}_k^{\pm}(\omega\pm i\epsilon)$ and $\varrho_k(\omega)$ one should account also for the poles of Fermi function $n(\omega)$ in the plane of complex ω (so-called Matzubara frequencies):

$$\hbar\omega_n=\mu \pm i\pi T(2n+1), \quad n=0,1,2,\ldots. \quad \text{(A5)}$$

In principle, the sum extends over infinitely many terms, but in practice the summation in Eq. (4.2) is cut at such frequencies ω_n which contribute less than determined by the desired accuracy.

[1] V.M. Strutinsky, N.Ya. Lashchenko, and N.A. Popov, Nucl. Phys. **46**, 639 (1963).
[2] V.S. Stavinsky, N.S. Rabotnov, and A.A. Seregin, Yad. Fiz. **7**, 1051 (1968) [Sov. J. Nucl. Phys. **7**, 631 (1968)].
[3] V.V. Pashkevich, Nucl. Phys. **A169**, 275 (1971).
[4] S. Yamaji, F.A. Ivanyuk, and H. Hofmann, Nucl. Phys. (submitted).
[5] A. Bohr and B. Mottelson, *Nuclear Structure* (Benjamin, London, 1975), Vol. 2.
[6] R. Samhammer, Ph.D. thesis, Technical University Munich,

1988; R. Samhammer, H. Hofmann, and S. Yamaji, Nucl. Phys. **A503**, 404 (1989).
[7] T. Wada, N. Carjan, and A. Abe, Nucl. Phys. **A538**, 283c (1992); Phys. Rev. Lett. **70**, 3538 (1993).
[8] K. Pomorski, J. Bartel, J. Richert, and K. Dietrich, Nucl. Phys. **A605**, 87 (1996).
[9] I.I. Gontchar and P. Fröbrich, Phys. At. Nuclei **57**, 1181 (1994).
[10] M. Thoennessen, Nucl. Phys. **A599**, 1 (1996).
[11] J. Damgaard, H.C. Pauli, V.V. Pashkevich, and V.M. Strutinsky, Nucl. Phys. **A135**, 432 (1969).
[12] V.M. Strutinsky, Nucl. Phys. **A95**, 420 (1967); **A122**, 1 (1968).
[13] M. Brack, J. Damgaard, H.C. Pauli, A.S. Jensen, V.M. Strutinsky, and C.Y. Wong, Rev. Mod. Phys. **44**, 420 (1972).
[14] C. Guet, E. Strumberger, and M. Brack, Phys. Lett. B **205**, 427 (1988).
[15] P.J. Siemens and A.S. Jensen, *Elements of Nuclei: Many-Body Physics with the Strong Interaction* (Addison-Wesley, New York, 1987).
[16] H. Hofmann, Phys. Rep. (in press).
[17] D. Kiderlen, H. Hofmann, and F.A. Ivanyuk, Nucl. Phys. **A550**, 473 (1992).
[18] H. Hofmann, F.A. Ivanyuk, and S. Yamaji, Nucl. Phys. **A598**, 187 (1996).
[19] H. Hofmann, Phys. Lett. **61B**, 423 (1976).
[20] H. Hofmann, R. Samhammer, and S. Yamaji, Phys. Lett. B **229**, 309 (1989).
[21] W.J. Swiatecki, Nucl. Phys. **A574**, 233c (1994).
[22] H. Hofmann and F.A. Ivanyuk, Z. Phys. A **344**, 285 (1993).
[23] R. Alkofer, H. Hofmann, and P.J. Siemens, Nucl. Phys. **A476**, 213 (1988).
[24] S. Yamaji, H. Hofmann, and R. Samhammer, Nucl. Phys. **A475**, 487 (1988).
[25] A.S. Jensen, J. Leffers, H. Hofmann, and P.J. Siemens, Phys. Scr. **T5**, 186 (1983).
[26] J. Blocki, Y. Boneh, J.R. Nix, J. Randrup, M. Robel, A.J. Sierk, and W.J. Swiatecki, Ann. Phys. (N.Y.) **113**, 330 (1978).
[27] F.A. Ivanyuk, V.M. Kolomietz, and A.G. Magner, Phys. Rev. C **52**, 678 (1995).
[28] K.T.R. Davis, A.J. Sierk, and J.R. Nix, Phys. Rev. C **13**, 2385 (1976).
[29] F.A. Ivanyuk and K. Pomorski, Phys. Rev. C **53**, 1861 (1996).
[30] H. Hofmann, S. Yamaji, and A.S. Jensen, Phys. Lett. B **286**, 1 (1992).
[31] F.A. Ivanyuk and V.M. Strutinsky, Z. Phys. A **293**, 337 (1979).
[32] D. Hilscher, I.I. Gontchar, and H. Rossner, Phys. At. Nuclei **57**, 1187 (1994).
[33] D.J. Hofman, B.B. Back, I. Diószegi, C.P. Montoya, S. Schadmand, R. Varma, and P. Paul, Phys. Rev. Lett. **72**, 470 (1994); see also P. Paul and M. Thoennessen, Annu. Rev. Nucl. Part. Sci. **44**, 65 (1994).
[34] J.P. Lestone, in *Tours Symposium on Nuclear Physics II*, edited by H. Utsunomiya (World Scientific, Singapore, 1995); see also J.P. Lestone, Phys. Rev. Lett. **70**, 2245 (1993).